Predicting onset of high speed gas metal arc weld bead defects using dimensional analysis techniques

T. C. Nguyen[1,2], D. C. Weckman*[1] and D. A. Johnson[1]

The onset of geometric defects such as humping or discontinuous weld beads during gas metal arc welding (GMAW) frequently limits the use of higher welding speeds and increased productivity. In the present study, a dimensional analysis of the GMAW process was performed in order to identify a number of dimensionless groups formulated based on various GMAW process parameters and material properties that could be used to predict when humping or discontinuous weld beads would occur. Experimental data from bead on plate GMA welds in plain carbon steel plate made using argon and two different reactive shielding gases, welding powers between 5 and 12 kW and a range of welding speeds were then used to create dimensionless process maps. These maps showed the limiting welding speed above which the high speed weld defects occurred as a function of all influential process parameters. It was shown that all experimental data for limiting welding speeds could be collapsed onto two collinear dimensionless curves. Also, the transition from spray to rotational metal transfer was found to occur at a well defined value of one of these dimensionless parameters. The effects of workpiece preheat temperature on humping were correctly predicted and there was a good correlation between the dimensionless GMAW process map and experimental data from other independent studies. These results suggest that the occurrence of high speed weld bead defects such as humping and discontinuous weld beads as well as the transition from spray to rotational metal transfer can be predicted using these new dimensionless GMAW process maps.

Keywords: Gas metal arc welding, Weld bead defects, High speed, Dimensional analysis

Introduction

Since its invention in the late 1940s, the gas metal arc welding (GMAW) process has become the most commonly used non-autogenous welding process in a wide range of manufacturing industries such as the construction, shipbuilding, automotive, aerospace and petrochemical industries.[1–4] The GMAW process is used for a wide range of manual and automatic welding applications.[4] It is used in joining most commercial metals and alloys of similar or dissimilar composition and is generally one of the most economical, efficient and versatile fusion welding processes for permanently joining engineering alloys.[1]

As illustrated in Fig. 1, in the GMAW process, a welding power supply is used to create an electric arc between the workpiece and a consumable electrode wire which is fed through the contact tip in the welding torch and into the weld pool at a preset wire feedrate (WFR). As the torch is moved along the weld joint at a constant welding speed v_{ws}, the arc melts both the electrode wire and part of the workpiece at the joint interface. Molten metal from the tip of the electrode wire is transferred across the arc to the weld pool, thereby providing filler metal to fill the joint gaps and create the desired weld bead profile. There are four basic filler metal transfer modes: short circuiting, globular, spray and rotational transfer.[3,4] The transfer mode is influenced by various GMAW process parameters including welding current I, welding voltage V, electrode diameter $\varnothing_e$, electrode composition, electrode extension, contact tip to workpiece distance (CTWD) and shielding gas composition.[1–3] Shielding of the molten metal from the atmosphere is provided by using an inert gas such as argon, a reactive gas such as CO_2 or various mixtures of Ar, CO_2, O_2 and He. The GMAW process is a multivariate process with many synergistic interactions between the numerous process parameters. This has made it difficult to develop comprehensive and reliable models of the process that might be used to predict the effects of various preset

[1]Department of Mechanical Engineering, University of Waterloo, Waterloo, Ontario N2L 3G1, Canada
[2]Now at School of Engineering and Information Technology, Conestoga College, 299 Doon Valley Dr., Kitchener, Ontario N2G 4M4, Canada

*Corresponding author, email dweckman@mecheng1.uwaterloo.ca

Published by Maney on behalf of the Institute
Received 24 August 2006; accepted 17 August 2007
DOI 10.1179/174329307X236797

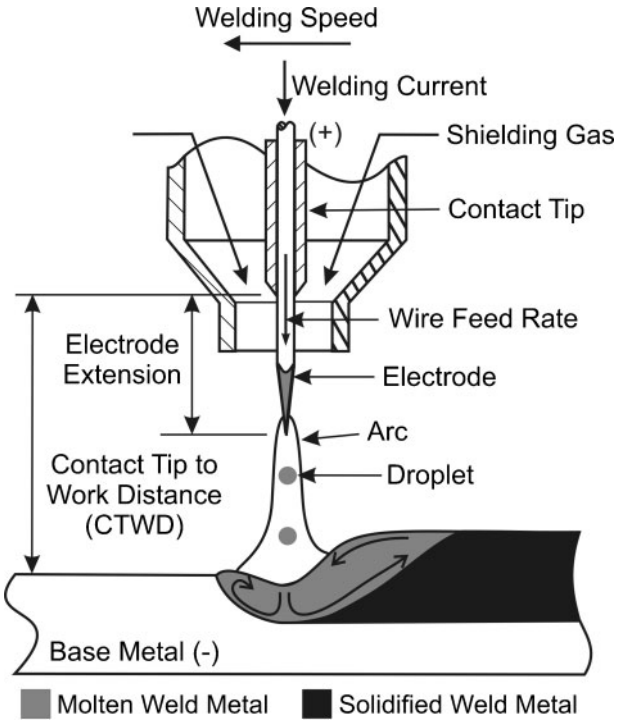

1 Schematic diagram of GMAW process in spray metal transfer mode

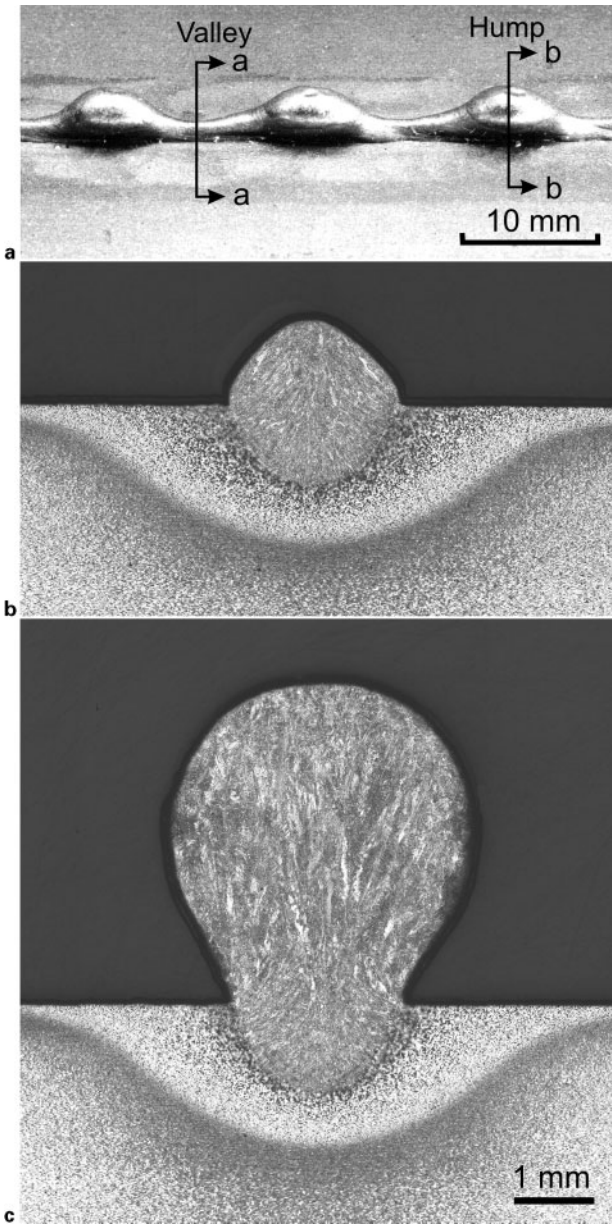

a top view; *b* transverse section of weld at valley; *c* transverse section at hump

2 Bead on plate GMA weld in AISI 1018 plain carbon steel exhibiting humping weld defect

weld process parameters on the resultant weld characteristics such as width, depth, weld bead shape, etc.

To remain competitive in today's manufacturing environment, companies must continuously improve their productivity without sacrificing the quality of their products. An increase in productivity often requires the use of higher welding speeds; however, the heat input must also be increased to maintain the same energy input per unit length of weld required for melting of the filler and base metals and to keep the same weld dimensions.[1,5,6] An unbounded increase in the welding speed and welding power is in practice not possible, because it is invariably limited by the deterioration of the quality of the weld bead profile and generation of weld bead defects. One of the most commonly occurring geometric defects that have been observed at high welding speeds is the humping phenomenon.[7–9] An example of a humped GMA weld bead is shown in Fig. 2. Humping can be described as a periodic undulation of the weld bead with humps and valleys. Figure 2*b* and *c* shows the transverse sections at a valley and a hump respectively of the humped GMA weld bead in Fig. 2*a*. The humping defect compromises the mechanical integrity of the weld joint, thereby limiting the welding speed and thus overall production rates. Humping has been reported to occur in both non-autogenous welding processes such as GMAW[10–13] and autogenous processes such as gas tungsten arc welding (GTAW),[14,15] laser beam welding (LBW)[16,17] and electron beam welding (EWB).[18–20]

Several phenomenological models of humping have been proposed in attempts to explain the physical mechanisms responsible for humping in autogenous and non-autogenous welding processes.[10,14,21–24] Nguyen *et al.*[13] have recently proposed the curved wall jet model of humping in high speed GMAW which is illustrated in Fig. 3. They argued that the combined actions of the arc force and the momentum of the droplets from the electrode create a gouged region at the front of the weld pool. These actions push the liquid metal to the back of the weld pool through a curved wall jet where it accumulates and grows into a swelling or humped bead as shown in Fig. 2*a* and *c*. Periodically, solidification of the long, narrow curved wall jet chokes off flow of molten metal to the swelling and a new swelling begins to form further along the weld bead. While models such as these are attempting to describe the physical phenomenon responsible for humping and helping to identify the weld process parameters that may cause humping, they cannot be used to quantitatively predict under what conditions humping will occur.

When GMA welds were made using the reactive shielding gases and higher welding powers, Nguyen

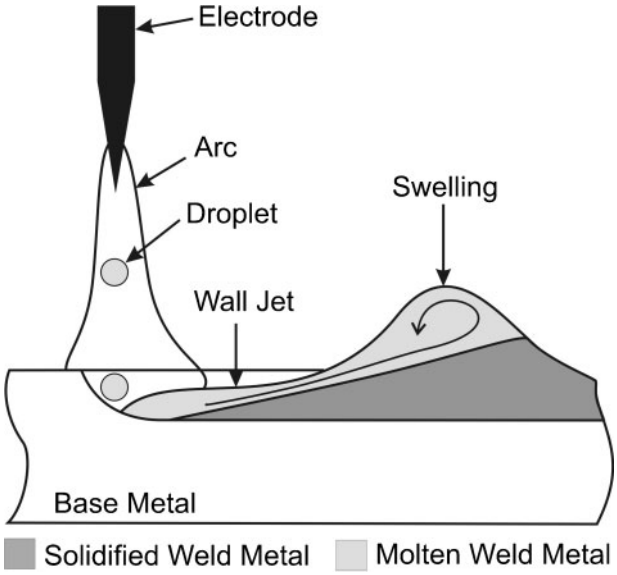

3 Curved wall jet model for humping during high speed GMAW (after Nguyen *et al.*[8,13,26])

et al.[25,26] observed a transition from spray to rotational metal transfer and a new type of weld defect which they called the discontinuous weld bead defect. Figure 4 shows a discontinuous GMAW weld bead. The regular periodic behaviour of humping is no longer evident, rather, there are segments of good weld beads that are interrupted at random intervals along the length of the weld bead by depressions in the base metal where the base metal has been melted and gouged but no weld or filler metal is present.

Nguyen *et al.*[25,26] attributed the formation of the aperiodic discontinuous weld bead defect to the inconsistent transfer of the molten filler metal from the electrode wire to the weld pool when welding in rotational transfer mode with reactive shielding gases. For example, Fig. 5*a* is a LaserStrobe video image[27] of the rotational transfer mode with the filler metal detaching as droplets or fragments from a characteristically long molten metal string on the end of the electrode. Occasionally, a very long fragment or all of the molten metal string on the end of the electrode will detach as shown in Fig. 5*b*. While the welding arc is still present, this temporary disruption of the transfer of the molten filler metal into the weld joint results in a depression or section where the weld bead has been arc gouged, but no filler metal deposited.

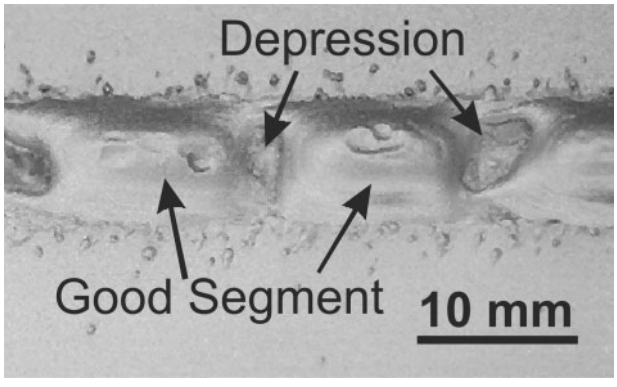

4 Top view of bead on plate GMA weld showing discontinuous weld bead defect

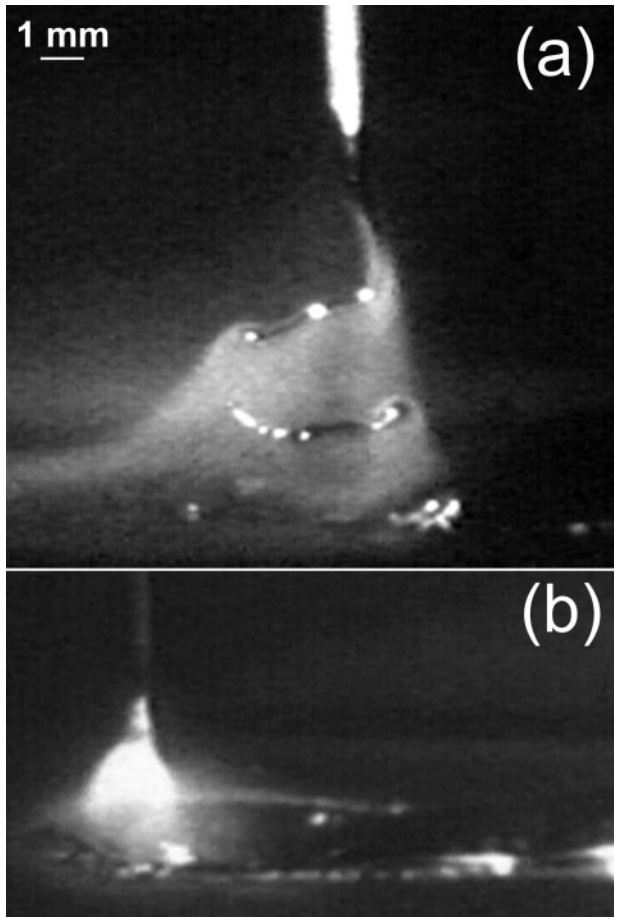

***a* detachment of long molten metal string fragment; *b* complete detachment of molten metal filament and welding without filler metal transfer during formation of depression**

5 LaserStrobe video images of rotational metal transfer during formation of discontinuous weld bead defect

In their studies of high speed weld bead defects in the GMAW process, Nishiguchi *et al.*[11,12] and Nguyen *et al.*[13,25,26] have developed parametric maps of welding current or power versus welding speed that show regions of process parameters that produced good weld beads and regions or conditions that resulted in humping and other weld defects. For example, Fig. 6 is a process map that consolidates the limiting welding speed data developed by Nguyen *et al.*[13,25,26] during their studies of humping and discontinuous weld bead defects in GMA welds in AISI 1018 plain carbon steel. The plot shows regions of welding power and welding speed that resulted in good and defective weld beads when using argon, Mig Mix Gold (MMG) (Praxair Distribution Inc., Kitchener, ON, Canada) (Ar–8CO_2) and TIME (BOC Gases Canada Ltd, Waterloo, ON, Canada) (Ar–8CO_2–26·5He–0·5O_2) shielding gases. In this plot, the lines represent the maximum or limiting welding speeds that could be used to produce a GMA weld without a defective weld bead profile. From this plot, the limiting welding speed was a function of the shielding gas, the welding speed and the welding power. When using the MMG and TIME reactive shielding gases and the welding power of <9 kW, the usable welding speed was limited by the occurrence of humping.[13,26] The limiting welding speed was significantly less when using argon shielding gas. With the welding power of >9 kW, welds

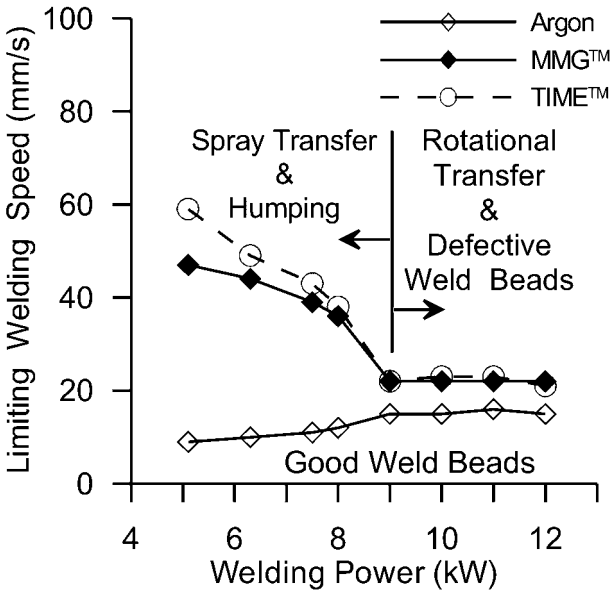

6 Dimensional plot of limiting welding speeds before onset of humping or discontinuous weld bead defects in GMA welds made in AISI 1018 plain carbon steel versus welding power when using argon, MMG and TIME shielding gases (taken from Nguyen *et al.*[13,25,26])

made using the argon shielding gas exhibited humping, whereas, the discontinuous weld bead defect was observed when using the reactive shielding gases and there was a distinct point of inflection between the limiting welding speed lines for humping versus the discontinuous weld bead defect. This point of inflection and change in behaviour at welding powers >9 kW is indicative that a transition has taken place in the physical phenomena taking placing during the GMAW including a change in the filler metal transfer mechanism from spray to rotational transfer.

While weld process maps such as that shown in Fig. 6 are valuable in identifying relationships and trends between the various controllable process parameters, they are of limited value in predicting when humping will occur in new applications because all preset welding process parameters such as the shielding gas composition, the torch angle, CTWD, $\varnothing_e$, electrode composition, etc., are kept constant when generating these process maps. A change of any one of these preset parameters would invalidate the process map and necessitate an expensive and time consuming series of experiments to generate a new process map. Since the GMAW process is a multivariate process with many independent parameters, the number of experiments required to fully explore the interactions between these parameters and the formation of high speed weld defects quickly becomes too large and impractical to perform.[28,29] In such cases, it is advantageous to employ a dimensional analysis technique to reduce the dimensionality of the problem and the number of experiments required, without obscuring possible relationships between the process parameters and the onset of the high speed weld defects.[30]

In their study of humping in GTA welds in 304 stainless steel, Mendez *et al.*[22–24] have performed a dimensional analysis on specific aspects of the humping phenomena and an order of magnitude scaling study in order to identify the most important parameters and physical phenomenon responsible for humping and also to try to predict under what conditions humping will occur. In the context of the present study of high speed weld bead defects in GMAW; however, the use of dimensional analysis has other advantages. For example, it is difficult to properly illustrate, visualise and interpret the effects of all process parameters on the onset of high speed weld defects using multidimensional plots. If these process parameters can be combined into dimensionless groups, then their combined effects can sometimes be shown simultaneously on two-dimensional plots, thereby reducing the dimensions of the problem. Thus, the dimensional analysis may provide a better method to characterise and understand the relationship between the various GMAW process parameters and the onset of high speed weld defects.

The objective of the present study[26] was to gain an insight into the physical parameters responsible for the formation of high speed GMA weld bead defects by performing a dimensional analysis of the high speed weld defect phenomena. One of the primary goals of this analysis was to identify combinations of dimensionless parameters that would collapse all dimensional welding results shown in Fig. 6 onto a single dimensionless line or value representative of the dimensionless limiting welding speed thereby facilitating the prediction of the occurrence high speed GMA weld defects. This work was performed in conjunction with the experimental data from Nguyen *et al.*'s[13,25,26] previously reported studies of high speed GMA weld defects.

Experimental apparatus and procedures

The experimental data used for the present dimensional analysis were obtained from bead on plate GMA welds that were made using a Fanuc ARC Mate 120i 6-axis welding robot and a Lincoln PowerWave 455 power supply operating in constant voltage mode. Welds were made using a wide range of preset welding speeds and welding powers. Using a preset constant voltage, different welding powers were obtained by varying the WFR until the desired welding current was realised. All welds were made using either spray or rotation metal transfer. A PC microcomputer was used with Labview software and National Instruments based data acquisition system to record the welding voltages V and currents I. These were then used to calculate the time averaged welding power P using $P=VI$. Finally, a LaserStrobe video imaging system[27] was used to record images of the periodic humping and aperiodic discontinuous weld bead phenomena during GMAW.

All bead on plate GMA welds were made in the flat position on 6·5 mm (¼″) thick cold rolled SAE-AISI 1018 plain carbon steel plates using 0·9 mm (0·035″) diameter ER70S-6 electrode wire and a 22 mm CTWD. In all cases, the working angle of the GMAW torch was 90° and the travel angle was 0°. Three different shielding gases were used: argon, MMG and TIME. The composition of each shielding gas is listed in Table 1. More comprehensive descriptions of the experimental apparatus and procedures used may be found in Nguyen *et al.*[13,25,26]

Procedure for formulating dimensionless groups

In dimensional analysis, all relevant process parameters are assembled into groups of variables which are

dimensionless. According to Buckingham's theorem,[30] the number of dimensionless groups necessary to completely describe any physical system is equal to the number of controlling parameters minus the number of fundamental dimensions used in that system. In this study of the GMAW process, the fundamental dimensions are mass (kg), length (m), time (s), temperature (K) and current (A). Based on these fundamental dimensions and Buckingham's theorem,[30] the total number of dimensionless variables that can completely describe an observed physical phenomenon will always be equal to the number of process controlling parameters minus five. Therefore, dimensional analysis will always reduce the dimensionality of the problem as well as the number of experiments required.

In dimensional analysis, the formalised procedure used for formulating the various dimensionless groups from different process parameters has three major steps:[30,31]

(i) identify the dependent and the physically relevant independent process parameters
(ii) assemble the process parameters into various dimensionless groups and finally
(iii) express the dimensionless groups in combinations of well recognised dimensionless numbers.

Dependent and independent dimensional variables

In the first step of any dimensional analysis, it is essential to clearly identify dependent and physically relevant independent dimensional variables of the process. To be successful, however, thorough knowledge of the process and of the observed physical phenomenon is needed to correctly identify suitable dependent dimensional variables and to critically evaluate the physical relevancy of different independent dimensional variables. An independent variable is physically relevant if it has a significant influence on the final value of the selected dependent variable.[30] If a physically relevant independent variable is overlooked or omitted, then the final results will be very confusing and difficult to interpret.

In any dimensional analysis, the dependent variable must be a measurable quantity that represents a certain aspect of the observed phenomenon. For example, there is a welding speed beyond which high speed weld bead defects will occur. As shown in Fig. 6, this limiting welding speed is strongly dependent on various process parameters such as the power input and the shielding gas composition. Since the objective of a GMAW procedure development exercise is normally to achieve the highest possible welding speed, the limiting welding speed v_l (m/s) would be a suitable dependent variable.

Possible physically relevant and independent variables in the dimensional analysis are the GMAW process parameters, the initial condition of the workpiece and the material properties of the workpiece. The GMAW process parameters that are physically relevant or that are known to have strong influences on the limiting welding speed are the welding voltage V (Volts or in fundamental dimensions, $m^2\ kg\ s^{-3}\ A^{-1}$), the wire feed speed (WFS) (m/s), the CTWD (m), the diameter of the filler metal electrode $\varnothing_e$ (m), the shielding gas composition and the electrical resistivity of the filler metal r (Ω m or in fundamental dimensions, $m^3\ kg\ s^{-3}\ A^{-2}$). In the present study, the electrical resistivity of the filler metal is similar to that of the workpiece.

Nguyen *et al.*[13,25,26] found that the shielding gas composition affects the arc current and power, arc length, the surface tension of molten metal in the weld pool and the area over which the molten filler metal droplets impinged the weld pool surface. These were all shown to affect the limiting welding speed. As such, the shielding gas composition is deemed to be a physically relevant independent variable. Initially, the surface tension γ (N m^{-1} or kg s^{-2}) of the molten weld metal can be used to quantitatively represent the overall effects of the shielding gas in the dimensional analysis. However, the arc length l_{arc} (m) and the weld width w_w (m) were also used, especially when considering the spray transfer mode of GMAW. For the purpose of this dimensional analysis, the surface tension of molten steel in GMAW when using ER70S-6 electrode material and different shielding gas compositions have been taken from the work of Subramaniam and White.[32] These surface tensions are summarised in Table 2.

In the list of influential GMAW process parameters discussed above, the welding current I (A) was purposely left out since the Lincoln PowerWave 455 power supply was used in the constant voltage mode throughout the study.[13,25,26] In the constant voltage mode, the welding current is a dependent variable and a consequence of the combination of shielding gas composition V, WFR, CTWD, $\varnothing_e$ and r.[1] If I (A) is included with the other independent process parameters, there will be a redundancy created which may obscure the actual relationships between various GMAW process parameters and the onset of the high speed weld defects. Nevertheless, I (A) can be used to represent the combined effects of shielding gas composition, WFR, CTWD, $\varnothing_e$ and r on v_l (m/s). In other words, by using I (A), the number of independent dimensional variables is reduced by three in the dimensional analysis. In addition, multiplication of V (V) and I (A) can be used to represent the power P (W or kg $m^2\ s^{-3}$), generated during welding.

The remaining independent dimensional variables are the initial temperature of the workpiece T_o (K) and the material properties of the SAE-AISI 1018 plain carbon steel workpiece. The initial temperature of the workpiece is a physically relevant independent variable since it has been experimentally demonstrated that the limiting welding speed in GMAW of plain carbon steel increases as the initial temperature of the workpiece is increased.[33] In this dimensional analysis, the initial temperature of

Table 1 Compositions of GMAW shielding gases used

Shielding gas	Composition
Argon	100%Ar (Ultra high purity grade)
MMG	92%Ar, 8%CO_2
TIME	65%Ar, 8%CO_2, 26·5%He, 0·5%O_2

Table 2 Surface tension of molten steel in GMAW with different shielding gas compositions[32]

Shielding gas	Surface tension, N m^{-1}
Pure argon	1·56
MMG	1·15
TIME	1·15
Pure CO_2	1·20
Argon and 5%O_2	1·15

the workpiece will be expressed as the temperature difference with respect to absolute 0 K, i.e. ΔT_o (K)=T_o (K)–0 K=T (K).

The material properties of the steel workpiece include thermal conductivity k (W m^{-1} K^{-1} or kg m s^{-3} K^{-1}), specific heat c_p (J kg^{-1} K^{-1} or m^2 s^{-2} K^{-1}), density ρ (kg m^{-3}) and electrical resistivity r (Ω m or m^3 kg s^{-3} A^{-2}). During welding, there is a large temperature gradient along the GMA electrode wire as the wire leaves the contact tip at room temperature and is heated to its melting point at the tip of the electrode. Similarly, a portion of the workpiece located directly underneath the welding arc will exceed the melting temperature, while the material at the edge of the workpiece may still be at room temperature. Since the material properties are temperature dependent, these large differences in temperature result in significant differences in the material properties throughout the workpiece and the electrode wire. In a dimensional analysis, a single value is normally required for a material property. Therefore, the material properties must be based on an appropriate average value of each specific material property over the temperature range experienced by the material.

Since the density of steel is a relatively weak function of temperature, a constant value of 7844 kg m^{-3} was used in the present study for all temperatures.[34] On the other hand, k, c_p and r of the steel are strongly affected by temperature.[34–36] An average value for k, c_p and r was obtained by numerically integrating their values between room temperature (293 K) and the melting point of steel (1800 K), and then divided by the temperature range, i.e.

$$\psi_{\text{average}} = \frac{\int_{293}^{1800} \psi(T) \times \mathrm{d}T}{1800-293} \tag{1}$$

where ψ_{average} is the average material property of interest and T is the temperature in degrees Kelvin. Thus, using the data published by Pehlke *et al.*,[34] the integrated average thermal conductivity of the steel is 35·6 W m^{-1} K^{-1}. Using the correlations between c_p and T obtained from Watt *et al.*,[35] the integrated average specific heat is 834·3 J kg^{-1} K^{-1}. Finally, the integrated average electrical resistivity of the steel is $7{\cdot}39 \times 10^{-7}$ Ω m.[36]

Table 3 contains a summary of the initial dependent and independent variables used in the present dimensional analysis. The dependent dimensional variable is v_l (m s^{-1}) while there are ten independent dimensional variables; V, WFS, CTWD, $\varnothing_e$, γ, T_o and the material properties k, c_p, ρ and r. Previously published experimental data often include welding power as a dependent variable. However, direct comparisons with these data cannot be made using the independent variables listed in Table 3, because the welding power cannot be explicitly represented in the dimensionless numbers generated by the dependent variable in this list. If the welding current is included in Table 3 as an independent variable, then it can be multiplied by the voltage to form the welding power. However, with the addition of I, the parameters WFS, CTWD, $\varnothing_e$ and r must be left out to avoid any redundancy. As shown in Table 3, the final list of independent process variables has been significantly reduced from ten to six. These are the power P (kg m^2 s^{-3}), γ (kg s^{-2}), ΔT_o (K), c_p (m^2 s^{-2} K^{-1}), k (kg m s^{-3} K^{-1}) and ρ (kg m^{-3}). Note that by using the welding power P as an independent process variable, the fundamental dimension of current (A) is no longer required in the analysis.

Assembling dimensionless variables

In dimensional analysis, the 'π' label with numerical subscript is traditionally used to represent a dimensionless group of variables. In this case, according to the Buckingham's theorem,[30] with seven dimensional variables and four fundamental dimensions, there will be three dimensionless groups: π_1, π_2 and π_3. To assemble or form a dimensionless group of welding parameters, π_0 for example, v_l, will be grouped with ΔT_o, c_p, k and ρ, since these independent variables contain the fundamental dimensions (i.e. kg, m, s and K) that are suitable to form the foundation for each dimensionless group. Physically, π_0 can be interpreted as a dimensionless limiting welding speed. Initially, the exponent of each dimensional variable in the group is unknown and can be expressed mathematically as

$$\pi_0 = (v_l)^{x_1}(\Delta T_o)^{x_2}(k)^{x_3}(c_p)^{x_4}(\rho)^{x_5} \tag{2}$$

where x_1–x_5 are the unknown exponents and the dimensional variables v_l, ΔT_o, c_p, k and ρ are as previously defined. Since the unit of each dimensional variable can be expressed in terms of fundamental dimensions of mass (kg), length (m), time (s) and temperature (K), the overall dimension of equation (2) is

$$[\pi_0] = \left(\frac{\mathrm{m}}{\mathrm{s}}\right)^{x_1}(\mathrm{K})^{x_2}\left(\frac{\mathrm{kgm}}{\mathrm{s^3K}}\right)^{x_3}\left(\frac{\mathrm{m^2}}{\mathrm{s^2K}}\right)^{x_4}\left(\frac{\mathrm{kg}}{\mathrm{m^3}}\right)^{x_5} = \mathrm{kg^0m^0s^0K^0} \tag{3}$$

where $[\pi_0]$ refers to the dimension of π_0.

Table 3 Summary of dependent and independent variables used in dimensional analysis

Dependent variable	Initial set of independent variables	Final set of independent variables
Limiting welding speed v_l	Voltage setting V WFS CTWD Diameter of electrode wire $\varnothing_e$ Effects of shielding gas as represented by the surface tension of the molten metal γ, the arc length l_{arc} and the weld width w_w Initial temperature of the workpiece T_o Thermal conductivity k Specific heat c_p Density ρ Electrical resistivity r	Welding power P Effects of shielding gas as represented by the surface tension of the molten metal γ, the arc length l_{arc} and the weld width w_w Initial temperature of the workpiece T_o Thermal conductivity k Specific heat c_p Density ρ

As indicated in equation (3), the sum of the exponents of each fundamental dimension m, kg, s and K must equal 0 since π_0 is dimensionless. This requirement results in the creation of four simultaneous equations with five unknown exponents. To solve for the exponents, x_1 is often assumed equal to 1 and the simultaneous equations can then be used to solve for the remaining exponents. Once the exponents are known, the dimensionless group π_0 can be assembled according to equation (2).

The procedure required to form one dimensionless group can be long, mathematically cumbersome and prone to arithmetic errors. To speed up the process and to minimise the chance of obtaining erroneous solutions, a more concise, algebraic based procedure of simultaneously forming several dimensionless groups has been developed.[30] A brief description of this procedure as applied to the current set of independent and dependent parameters is presented in the Appendix. The following dimensionless parameters were derived using this procedure and the seven dimensional process parameters listed in Table 3

$$\pi_1 = \frac{v_l}{(\Delta T_o \times c_p)^{1/2}} \tag{4}$$

$$\pi_2 = \frac{P c_p^{1\cdot5} \rho}{(\Delta T_o)^{1/2} k^2} \tag{5}$$

$$\pi_3 = \frac{\gamma (c_p)^{1/2}}{(\Delta T_o)^{1/2} k} \tag{6}$$

Recognising that the material properties and initial temperatures are preset constants, π_1 is representative of a dimensionless limiting welding speed and π_2 is a dimensionless welding power. Finally, π_3 may be thought of as a dimensionless number that represents the effects of shielding gas composition on the surface tension of the metal.

Expressing dimensionless groups in recognisable dimensionless numbers

The newly formed dimensionless groups in equations (4)–(6) can often be expressed as a combination of well recognised named dimensionless numbers. In the present example, π_1 contains v_l, ΔT_o and c_p. This dimensionless group contains the same variable types and has a similar form to the Eckert number Ec.[30] The Eckert number is the square of velocity divided by the product of the specific heat capacity and the temperature difference. Therefore, π_1 can be precisely expressed as

$$\pi_1 = \frac{v_l}{(\Delta T_o c_p)^{1/2}} = (\mathrm{Ec})^{1/2} \tag{7}$$

The Eckert number can be physically interpreted as the ratio of kinetic energy to the enthalpy of the material. Using this approach, the other dimensionless groups can also be expressed in terms of other recognised dimensionless numbers.

Results and discussion

Initial analysis

To determine if there are any correlations between the dimensionless groups π_1, π_2 and π_3, the experimental data from the previous studies by Nguyen *et al.*[13,25,26] were used to calculate the corresponding dimensionless numbers and these were then plotted and examined. For example, Fig. 7 contains the experimental data in a plot of π_1 versus π_3 where π_1 consists of the parameters v_l, c_p and ΔT_o while π_3 is a function of γ, c_p, ΔT_o and k (*see* equations (4) and (6)). If there is no correlation between π_1 and π_3, the data in Fig. 7 would be randomly distributed. However, the dimensionless group π_3 may be seen to stratify the data into two distinct groups. When π_3 is about 8×10^{-2}, the data points belong to the GMA welds produced using argon shielding gas. Meanwhile, the other data at about $\pi_3 = 6 \times 10^{-2}$ contain data from welds produced using the reactive shielding gases MMG or TIME. These results show the influences of the reactive shielding gases as reflected through the surface tension of molten weld metal. However, for a given value of π_3, i.e. reactive versus inert shielding gas, there is a great deal of scatter in the π_1 data and no clear correlation. Thus, the correlation between π_3 and π_1 is not very meaningful.

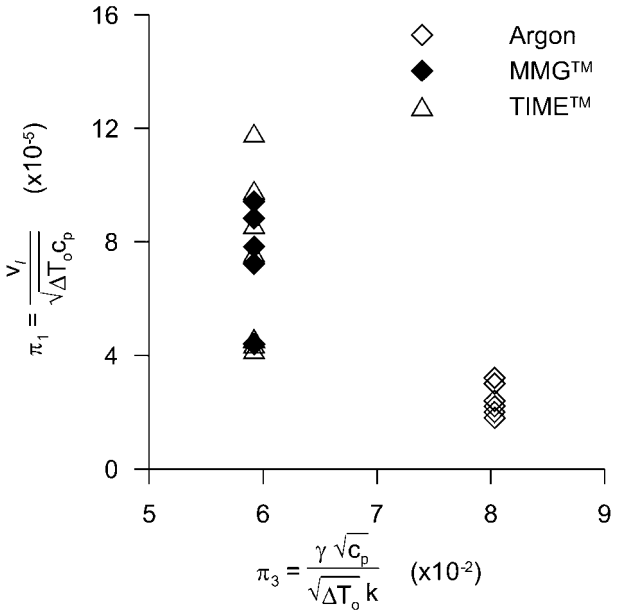

7 Relationships between dimensionless variables π_1 and π_3

Figure 8 shows a plot between dimensionless variables π_1 and π_2. The dimensionless variable π_2 includes the power $P = VI$, and the material properties ρ, ΔT_o, c_p and k. For each type of shielding gas, the line represents the boundary separating the good and the defective weld bead regions, i.e. the dimensionless limiting welding speed π_1. Good weld beads were produced in the region underneath each line while defective weld beads were produced in the region above each line. Note that Fig. 8 is identical in form to the dimensional plots of the dimensional experimental data in Fig. 6 because all other parameters in π_1 and π_2 are constants. Thus, the dimensionless limiting welding speed π_1 is a function of the dimensionless power π_2 and the shielding gas composition.

The relationships displayed in Fig. 8 were based on data generated using various welding powers while ΔT_o was constant. However, Finlayson[33] has shown that humping can be avoided by preheating the workpiece, i.e. by increasing ΔT_o. For example, Fig. 9*a* is the top

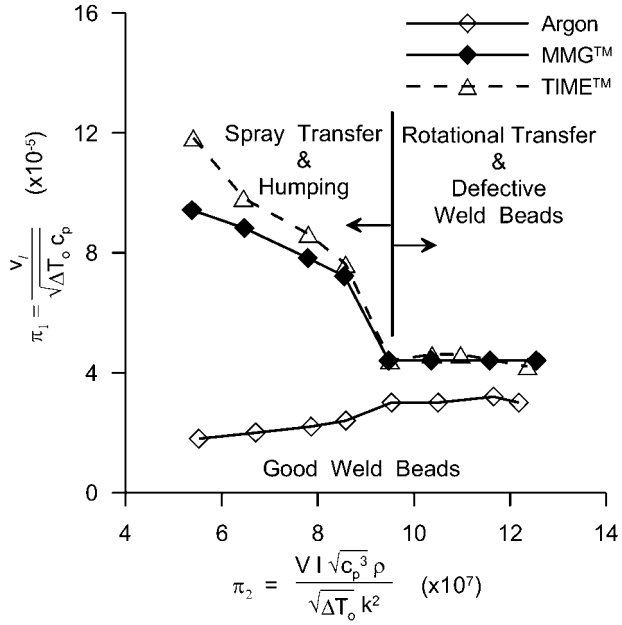

8 Correlation between dimensionless variables π_1 and π_2

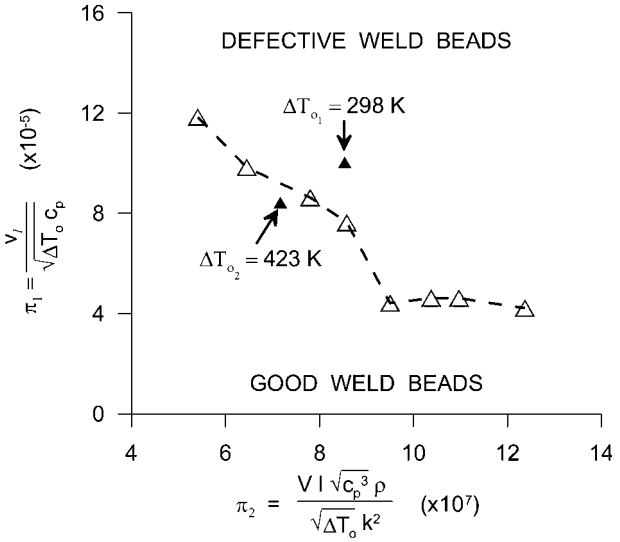

10 Effect of initial workpiece temperature on occurrence of high speed weld defects when using TIME shielding gas

view of a GMA weld exhibiting humping that was produced using TIME shielding gas, a welding speed of 50 mm s^{-1}, a welding power of 8·2 kW and an initial temperature of ΔT_{o1}=298 K (25°C) while Fig. 9*b* shows a good weld bead that was produced using the same welding parameters while preheating the workpiece to ΔT_{o2}=423 K (150°C). Using the welding process parameters for the weld made using ΔT_{o1}=298 K, the values of π_1 and π_2 are $10{\cdot}0\times10^{-5}$ and $8{\cdot}54\times10^{7}$ respectively. As shown in Fig. 10, this combination of π_1 and π_2 is clearly located in the defective weld bead region and is in agreement with the observed humped weld bead geometry (*see* Fig. 9*a*). Similarly, by preheating the workpiece to 423 K, the values of π_1 and π_2 become $8{\cdot}42\times10^{-5}$ and $7{\cdot}16\times10^{7}$ respectively. As shown in Fig. 10, these dimensionless numbers are correctly predicted to be in the good weld bead region. Thus, in their current form, π_1 and π_2 have correctly captured the influence of the initial temperature of the workpiece on the occurrence of the humping in GMA weld beads.

Revisions to initial analysis

As shown in Fig. 7, when the experimental data were plotted as π_1 versus π_3, there was no apparent correlation between these two dimensionless parameters other than the segregation of the π_3 data between the Ar and the other two reactive shielding gases. However, when plotted as π_1 versus π_2 (*see* Fig. 8), there appear to be correlations as the data fall along three distinct lines. Unfortunately, the dimensionless limiting welding speed lines shown in Fig. 8 are still segregated according to the type of shielding gas used. This suggests that our initial selection of influential dimensional process parameters used to derive π_1 and π_2 was incomplete and that the effects of all influential variables have not yet been included. Thus, further judicious revisions to these original dimensionless groupings are required to facilitate the collapse of these data onto a single dimensionless line.

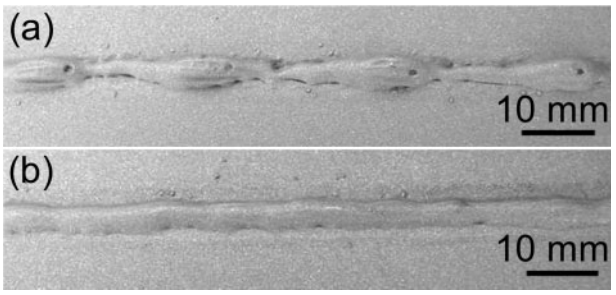

9 Top view of GMA welds produced with initial workpiece temperature of *a* 298 K (25°C) exhibiting humping and *b* 423 K (150°C) without humping

In Fig. 8, when π_2 is $>9{\cdot}5\times10^{7}$, the mode of filler metal transfer is rotational and π_1 for all shielding gases is independent of π_2. The limiting welding speeds of the reactive shielding gases are the same at about $\pi_1=4\times10^{-5}$. However, π_1 of the welds produced using argon shielding gas was consistently lower at about $\pi_1=3\times10^{-5}$. While the effects of shielding gas composition on the welding current and power have already been incorporated in π_2 through the inclusion of V and I, the effects of shielding gas composition on the surface tension of the molten metal has not yet been included. From Fig. 7, the dimensionless surface tension of the molten weld metal, π_3, appears to strongly influence π_1 by stratifying the experimental data into two groups. Perhaps, the observed separation in the current dimensionless plots is caused in part by the effect of the shielding gas on the surface tension of molten weld metal. To investigate this hypothesis, a new dimensionless variable is formed using the following equation

$$\pi_4=\pi_1\times\pi_3=\frac{v_l}{(\Delta T_o c_p)^{1/2}}\times\frac{\gamma(c_p)^{1/2}}{(\Delta T_o)^{1/2}k}=\frac{v_l\gamma}{\Delta T_o k} \qquad (8)$$

where π_1, π_3 and other dimensional variables are as previously defined.

Figure 11 is a plot of the new dimensionless variable π_4 versus the original dimensionless variable π_2. Note that π_4 includes the variables v_l, γ, ΔT_o and k. By combining the surface tension of the molten weld metal and the limiting welding speed into one dimensionless

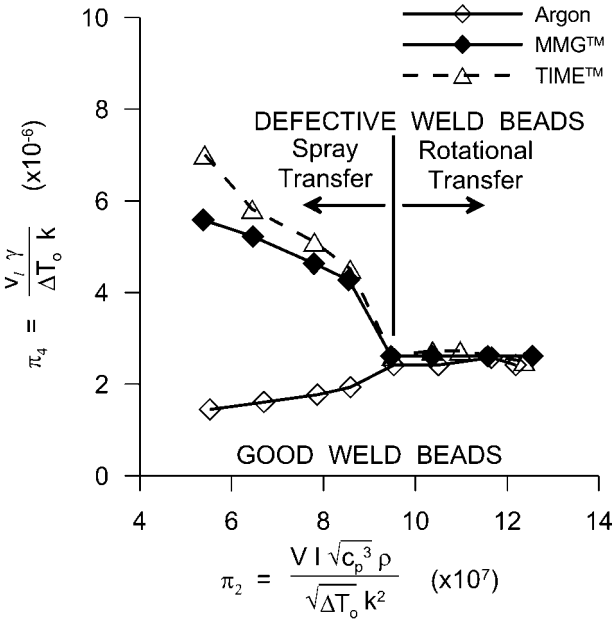

11 Plot of new dimensionless variables π_4 versus π_2

variable, the limiting welding speeds when using the different shielding gases merge into a single line when $\pi_2 \geq 9{\cdot}5 \times 10^7$ and rotational filler metal transfer mode occurred (*see* Fig. 11). Thus, high speed GMA weld bead defects are predicted to occur when $\pi_2 \geq 9{\cdot}5 \times 10^7$ and $\pi_4 \geq 2{\cdot}2 \times 10^{-6}$.

The collapse of the experimental data into a single curve $\pi_2 \geq 9{\cdot}5 \times 10^7$ strongly suggests that the previously observed separation in data was caused by the effect of shielding gas on the surface tension of the molten weld metal during rotational metal transfer. However, as shown in Fig. 11, including the effect of the shielding gas on the surface tension of the molten weld metal does not bring together the boundaries in the spray filler metal transfer region (when $\pi_2 \leqslant 9{\cdot}5 \times 10^7$). This suggests that other influential effects have not yet been included in the dimensionless variable π_4 in the spray transfer regime.

When welding using the same power and spray metal transfer, Nguyen *et al.*[13,25,26] found that in addition to the surface tension, the area over which the filler metal droplets impinged on the top surface of the weld pool and the arc length were strongly influenced by the shielding gas composition. Gas metal arc welds produced using reactive shielding gases had a shorter arc length and a larger filler metal droplet impingement area than welds produced with argon shielding gas. A short arc length reduces the distance over which the filler metal droplets can be accelerated by the arc plasma. As a result, the overall momentum of the filler metal droplets will be lower when they enter the weld pool thereby lowering the propensity for humping. Meanwhile, with the reactive shielding gases, the area over which the filler metal droplets enter the top surface of the weld pool is larger thereby spreading out the distribution of the incoming filler metal droplets. Based on the curved wall jet model of humping in GMAW[13,26] illustrated in Fig. 3, both of these effects will reduce the likelihood of creating a gouged weld pool surface and reduce the momentum of the backward flow of the molten weld metal, thereby suppressing the humping defect until higher welding speeds. However, these latter influences of the shielding gas have not yet been included in the dimensional analysis.

To include the additional effects of the shielding gas on the filler metal droplet impingement characteristics and the humping phenomenon during spray metal transfer, measurable quantities that represent the additional effects of the shielding gas must be included as physically relevant variables in the dimensional analysis. From the above observations, the arc length and the filler metal droplets impingement area are two variables that can quantify the additional influences of the shielding gas on the humping phenomenon. The arc length during GMAW was measured directly using the LaserStrobe video imaging system.[27] In addition, the area over which the filler metal droplets impinged on the top surface of the weld pools was measured. The filler metal droplet impingement area was found to correlate well to the weld width,[13,25,26] a quantity that can be more easily measured during or after welding. Consequently, in the present study, the weld width was used instead of the diameter of the filler metal droplet impingement area.

To examine the influences of shielding gas on the arc length and the weld width, different welding power levels must be used in the experiments. Since the arc length remains unchanged with higher welding speeds, it can be measured using the LaserStrobe video imaging system[27] at any welding speed, welding power and shielding gas combination. On the other hand, the weld width decreases with increasing welding speeds. Thus, proper welding speeds must be selected when making the weld width measurements.

The measured arc lengths and the weld widths are plotted against welding power in Fig. 12. The data are grouped according to the power levels. In addition, the plots also show the welding speeds at which these measurements were made. For instance, the welding speeds used to measure the arc length and weld width are 9, 10, 11 and 12 mm s^{-1} for 5, 6, 7·5 and 8 kW welding powers respectively. These welding speeds define the boundary between good and humped weld bead regions when using argon shielding gas. Again, with the exception of the shielding gases used, other GMAW process parameters were kept constant. From Fig. 12, argon shielded welds had longer arc lengths and narrower weld widths than those produced using the reactive shielding gases. Also, welds produced using the reactive shielding gas MMG had longer arc lengths and slightly narrower weld widths than those made using the TIME shielding gas.

Beyond the limiting welding speeds shown in Fig. 12, all argon shielded welds exhibited humping. At each limiting welding speed, the observed increase in arc length and decrease in weld width of the argon shielded welds relative to the welds made using the reactive shielding gases are representative of the effects of the shielding gases on the limiting welding speed. Since short arc length and wide weld width suppresses the onset of humping until higher welding speeds, these new variables are arranged as a ratio to modify the dimensionless variable π_4 as follows

$$\pi_5 = \pi_4 \times \frac{l_{\text{arc}}}{w_{\text{w}}} = \frac{v_{\text{l}}\gamma}{\Delta T_{\text{o}} k} \times \frac{l_{\text{arc}}}{w_{\text{w}}} \tag{9}$$

where l_{arc} is the arc length (m) and w_{w} is the weld width (m).

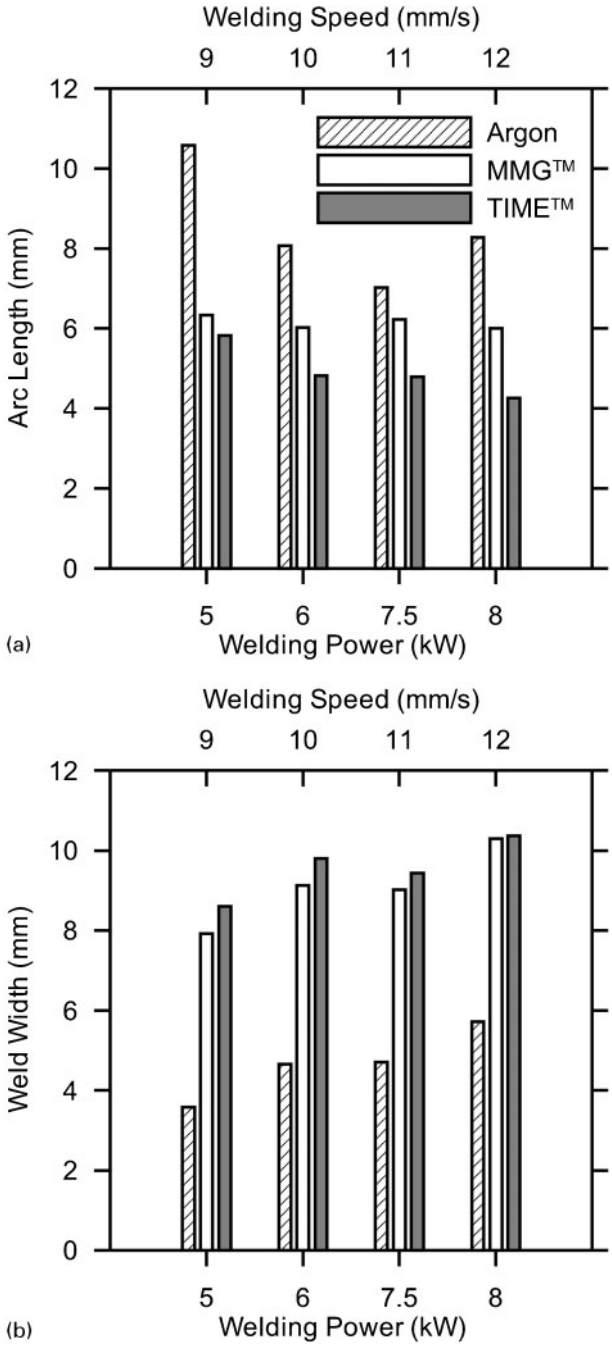

12 Plots of *a* arc length and *b* weld width versus welding power for different shielding gases and at different welding speeds

The arc length and the weld width were measured for each shielding gas and welding power level using the corresponding limiting welding speed of the argon shielded welds.

Thus far, all of the modifications of the dimensionless parameters have concentrated on the dimensionless limiting welding speed π_4, in order to account for the observed influences of the shielding gases on the dimensionless limiting welding speed. The dimensionless welding power variable π_2 has been left unaltered. As previously discussed, when π_2 is increased beyond $9{\cdot}5\times10^7$, the filler metal transfer mode switches from spray to rotational transfer. In other words, the transition from spray to rotational transfer mode apparently depends only on the welding power level. This is not

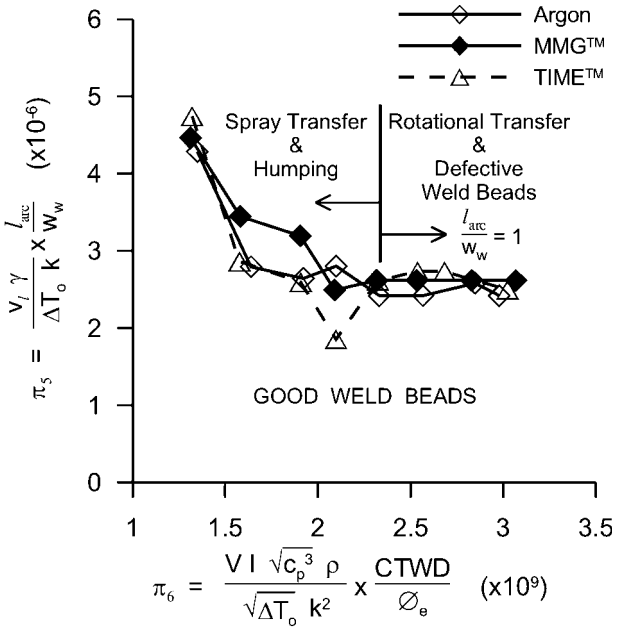

13 Plot of modified dimensionless variables π_5 and π_6

correct. The transition from spray to rotational transfer mode is known to be dependent not only on welding power, but also on the diameter of the filler metal electrode and the electrode stickout.[5] A long electrode stickout and a small electrode diameter will promote the transition from spray to rotational transfer modes at low welding currents or welding powers. The diameter of the filler metal wire is an independent process parameter selected before welding. On the other hand, the electrode stickout is the distance the electrode extends from the contact tip during welding (*see* Fig. 1). This is a dependent parameter. For each combination of shielding gas and welding power, the electrode stickout depends on the CTWD, an independent process parameter that is usually set before welding. Thus, instead of using the electrode stickout, the CTWD will be used in developing a new dimensionless number.

As previously explained, the welding current can be used to represent the combined effects of WFS, CTWD, $\varnothing_e$ and r. However, $\varnothing_e$ and CTWD also play a critical part in the transition from spray to rotational transfer modes. This is further evidence of the complex interactions and interdependence of the various GMAW process parameters. Therefore, in addition to the welding power, $\varnothing_e$ and CTWD (i.e. the electrode stickout) must also be included to properly account for the transition from spray to rotational filler metal transfer modes. With CTWD and $\varnothing_e$, the dimensionless variable π_2 can be modified to a new dimensionless variable π_6 as follows

$$\pi_6 = \pi_2 \times \frac{\mathrm{CTWD}}{\varnothing_e} = \frac{VI\left(c_p^3\right)^{1/2}\rho}{(\Delta T_o)^{1/2}k^2} \times \frac{\mathrm{CTWD}}{\varnothing_e} \qquad (10)$$

Figure 13 shows a plot of the weld data using the new dimensionless variables π_5 and π_6. In this plot, the transition from spray to rotational transfer occurs at $\pi_6 = 2{\cdot}3\times10^9$. For values of $\pi_6 < 2{\cdot}3\times10^9$ where spray transfer mode occurred, the inclusion of the ratio of l_{arc}/w_w in the dimensionless variable π_5 has removed the previously observed differences in the dimensionless

limiting welding speeds when using the different shielding gases and collapsed the data onto a single curve for limiting welding speed. Once the rotational transfer mode is achieved, however, the dimensionless limiting welding speed remains constant at $\sim 2{\cdot}6 \times 10^{-6}$ and becomes independent of π_6. For the rotational transfer mode, l_{arc}/w_w is set equal to 1 since the inclusion of the dimensionless surface tension term in π_5 has already been successful in merging the limiting welding speed lines of the different shielding gases (*see* Fig. 11). In other words, during the rotational transfer mode, the most significant influence of the shielding gas composition on the welding process appears to be its effect on the surface tension of the molten weld metal.

Forming dimensionless variables with recognisable dimensionless numbers

The dimensionless variables π_5 and π_6 can now be expressed in term of recognisable dimensionless numbers. Definitions and the physical interpretation of these well recognised dimensionless numbers may be found in Szires.[30] Using these, the dimensionless variable π_5 can be shown to consist of the Peclet (Pe), the Eckert (Ec) and the Weber (We) numbers, i.e.

$$\pi_5 = \frac{v_1 \gamma l_{arc}}{\Delta T_o k w_w} = \frac{PeEc}{We} \tag{11}$$

Similarly, π_6 can be expressed in terms of the Pe number, the Ec number and ξ_1, i.e.

$$\pi_6 = \frac{VI\left(c_p^3\right)^{1/2}\rho CTWD}{(\Delta T_o)^{1/2} k^2 \varnothing_e} = \frac{\xi_1 Pe}{(Ec)^{1/2}} \tag{12}$$

where ξ_1 is a dimensionless power input that is defined by the following equation[37]

$$\xi_1 = \frac{VI}{\Delta T_o k L} \tag{13}$$

ξ_1 was derived by Weckman *et al.*[37] by non-dimensionalising the Gaussian distributed surface heat flux boundary condition that is frequently used in modelling GTAW and LBW processes. In the present study, the characteristic length scale L in π_6 and ξ_1 is set equal to the diameter of the filler metal electrode $\varnothing_e$.

The Peclet number Pe in equation (12) can be physically interpreted as the ratio of heat transferred by bulk motion or advection of the base metal to the heat transferred in the base metal by conduction. It is expressed mathematically as[30]

$$Pe = \frac{v c_p \rho L}{k} \tag{14}$$

where v is the welding speed (m s^{-1}), L is a characteristic length (m), c_p, ρ and k are material properties. The Eckert number Ec is defined as[30]

$$Ec = \frac{v^2}{\Delta T_o c_p} \tag{15}$$

where ΔT_o is the temperature difference between the material and the surrounding (K). Finally, the Weber number We represents the ratio of the surface tension to the inertial force in a liquid and is defined as[30]

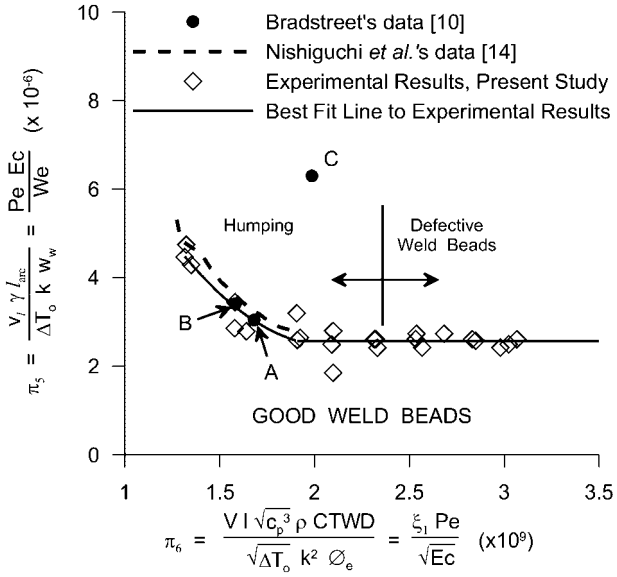

14 Dimensionless boundary between good and defective weld bead regions

$$We = \frac{v\rho^2 L}{\gamma} \tag{16}$$

Validating results of dimensional analysis

In Fig. 13, the good and the defective weld bead regions are separated by a boundary on a two-dimensional plot of two dimensionless parameters π_5 and π_6. Knowing this boundary, it is possible to predict whether a good or a defective weld bead would form based on the GMAW process parameters. However, to further ensure the reliability of the analysis, experimental data from other researchers can be plotted and compared against the results of the present study.

The results from GMAW experiments by Bradstreet[10] and Nishiguchi *et al.*[10] are plotted on the dimensionless plot of π_5 versus π_6 in Fig. 14. The solid circles represent three different humped welds produced by Bradstreet[10] using CO_2 (labelled C), argon (labelled B) and argon plus 5%O_2 (labelled A) shielding gases respectively. Meanwhile, the broken line is the limiting welding speed from Nishiguchi *et al.*'s[11] GMA welds with CO_2 as the shielding gas. Finally, in Fig. 14, best fit lines were determined using regression analysis and the limiting welding speed data from the present study. These are as follows

$$\pi_5 = (3{\cdot}2\pi_6^2 - 13{\cdot}6\pi_6 + 16{\cdot}8) \times 10^{-6} \quad \text{for} \quad \pi_6 < 1{\cdot}9 \times 10^9$$
$$\pi_5 = 2{\cdot}6 \times 10^{-6} \quad \text{for} \quad \pi_6 \geq 1{\cdot}9 \times 10^9 \tag{17}$$

with a coefficient of determination of 0·86. The boundary between these two lines and the humping and discontinuous weld bead defects occurs at $\pi_6 = 2{\cdot}3 \times 10^9$. This can also be considered as a transition point from spray to rotational filler metal transfer modes.

When plotting the experimental data from the works of Bradstreet[10] and Nishiguchi *et al.*[11] in Fig. 14, the value of π_5 was calculated based on the assumption that the ratio of the arc length to the weld width was unity.

This was necessary because the arc length and weld widths were not measured or reported. With this assumption, the experimental data from both Bradstreet[10] and Nishiguchi *et al.*[11] show good agreement with the data obtained from the present study. As may be seen from Fig. 14, the limiting welding speed from Nishiguchi *et al.*'s work[11] correlates well with the limiting welding speed obtained in the present dimensional analysis. Meanwhile, the humped GMA welds from Bradstreet's work[10] that were produced using argon or Ar–$5O_2$ shielding gas, lie on or above the limiting welding speed line obtained in the present dimensional analysis and are correctly predicted to exhibit humping. Meanwhile, the weld produced using CO_2 shielding gas and globular transfer is well within the humped weld bead region. Perhaps the welding speed of this humped weld was much greater than the limiting welding speed for this particular set of process parameters. The agreement between these three sets of experimental data suggests that the results of the dimensional analysis can be used with confidence to determine whether a good or a defective weld bead will be produced based on the values of the initial preset process parameters.

Second variation of dimensional analysis of high speed weld defects

During the formulation of the various dimensionless parameters, the dependent variable I (A) was used to represent the combined effects of shielding gas composition, WFS, CTWD, $\varnothing_e$ and r on the critical welding speed at which high speed weld bead defects would be produced. This substitution reduced the initial number of independent variables from ten to seven and successfully facilitated collapse of the data onto two collinear dimensionless lines (*see* Fig. 14 and equation (17)). This suggests that all important physical parameters responsible for the onset of high speed GMA weld bead defects have been included in these dimensionless parameters. However, the use of these dimensionless parameters as predictive tools is somewhat limited because I is a dependant parameter that must be measured from actual welds. The overall utility of the dimensional analysis as a predictive tool would be improved if the preset independent weld process parameters, WFS, CTWD, $\varnothing_e$ and r were used in place of I when formulating the dimensionless parameters. Thus, the dimensional analysis was performed again without substitution of the welding current and with instead WFS, CTWD, $\varnothing_e$ and r. From this analysis, a new dimensionless parameter π_7 was formed as follows

$$\pi_7 = \frac{V^2 \times \mathrm{WFS} \times \mathrm{CTWD} \times \varnothing_e \times \left(c_p \times \Delta T_m\right)^{1/2}}{r \times \Delta T_o \times k \times \alpha^2} = \frac{\xi_2 \mathrm{Pe}_{\mathrm{CTWD}} \mathrm{Pe}_{\varnothing_e}}{(\mathrm{Ec})^{1/2}} \quad (18)$$

As shown in equation (18), this new dimensionless variable π_7 can also be expressed as a combination of the Peclet numbers Pe, the Eckert number Ec and ξ_2. For the Pe number in the dimensionless parameter π_7, WFS is used for the velocity term. The $\mathrm{Pe}_{\mathrm{CTWD}}$ number has the CTWD as its characteristic length. Meanwhile, $\mathrm{Pe}_{\varnothing e}$ uses the diameter of the filler metal electrode as its characteristic length. Ec consists of WFS, ΔT_m and c_p.

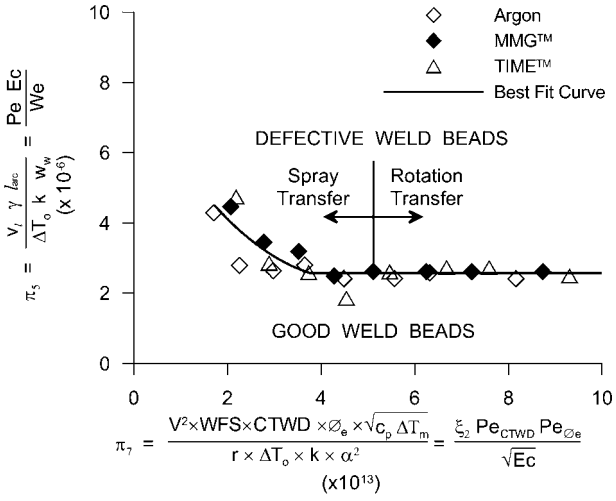

15 Dimensionless plot of π_5 versus π_7

Lastly, the term ξ_2 is defined as

$$\xi_2 = \frac{V^2}{r \Delta T_o k} \quad (19)$$

As before, ξ_2 can be interpreted as a dimensionless heat input term modelled after the dimensionless heat input term used by Weckman *et al.*[37]

A plot of the GMAW limiting welding speed data as functions of π_5 versus the new dimensionless parameter π_7 is shown in Fig. 15. In this plot, the dimensionless variable π_5 is as previously defined. When $\pi_7 = 5 \times 10^{13}$, the filler metal transfer mode changed from spray to rotational transfer. The results in Fig. 15 show the general trends previously observed in the results of earlier dimensional analysis. The limiting welding speed initially decreases with higher values of π_7. When π_7 is $> 3{\cdot}8 \times 10^{13}$, the dimensionless variable π_5 becomes independent of π_7 and equal to $2{\cdot}6 \times 10^{-6}$. The equations for the best fit limiting welding speed lines are

$$\pi_5 = (0{\cdot}3\pi_7^2 - 2{\cdot}3\pi_7 + 7{\cdot}7) \times 10^{-6} \quad \text{for} \quad \pi_7 < 3{\cdot}8 \times 10^{13}$$
$$\pi_5 = 2{\cdot}6 \times 10^{-6} \quad \text{for} \quad \pi_7 \geqslant 3{\cdot}8 \times 10^{13} \quad (20)$$

where π_5 and π_7 are as defined in the plot of Fig. 15 and the coefficient of determination is 0·7.

Although the trends observed in Fig. 15 are similar to those observed in the previous analysis, there is one advantage associated with this latter dimensional analysis. The dimensionless variable π_7 is now composed entirely of independent GMAW process parameters which are usually selected and preset before welding. From Fig. 15, users of the GMAW process can predict if defective weld beads will be made based on the selection of various preset welding parameters. Thus, from the user's point of view, the results of the latter dimensional analysis are of considerably more practical value. These results and the derived dimensionless variables provide valuable insights into possible welding techniques that could be used to weld at higher welding speeds without the occurrence of high speed weld bead defects.

Conclusions

Detailed observations of the sequence of events taking place during the formation of weld bead defects during high speed bead on plate GMAW of plain carbon steel

using Ar and two reactive shielding gases, MMG and TIME, have been used in conjunction with phenomenological models of humping and the discontinuous weld bead defect to perform a dimensional analysis of the process. Two dimensionless variables were developed using dimensional analysis techniques which were based upon preset process parameters. These dimensionless variables were then used with the experimental data to generate dimensionless weld process maps that documented the effect of different influential GMAW process parameters on the limiting welding speed and the onset of the two different high speed weld defects. The first dimensionless variable π_5 combined the limiting welding speed and the influences of the shielding gas, while the second dimensionless variable π_7 represented the welding power used during GMAW.

It was shown that the different limiting welding speed lines observed when plotting the dimensional experimental data could be collapsed onto two collinear dimensionless curves of π_5 versus π_7, one for the region in which spray metal transfer and humping occurred and the other for the region in which rotational transfer occurred and either humping or the discontinuous weld bead defect was observed. Also, the transition from spray transfer to rotational metal transfer was found to occur at a given value of π_7, thus, π_7 can also be used to predict when this transition will occur. Use of the dimensionless parameters reduced the dimensionality of the problem and allowed predictions of the occurrence of the high speed weld defects to be simultaneously related to various influential GMAW process parameters on one single two-dimensional plot.

The dimensionless parameters and process map were shown to correctly predict the observed effects of workpiece preheat temperature on the occurrence of humping. In addition, there was good correlation between the dimensionless GMAW process map and previously published experimental data from a number of independent studies. Thus, the occurrence of high speed weld defects such as humping or the discontinuous weld bead and the transition from spray to rotational metal transfer can be predicted for the first time using the predetermined value of various process parameters in conjunction with the dimensionless GMAW process map of π_5 versus π_7.

Appendix

The procedure required to form dimensionless groups can be long, mathematically cumbersome and prone to arithmetic errors. To speed up the process and minimise the chance of obtaining erroneous solutions, a more concise, algebraic based procedure of simultaneously forming several dimensionless groups has been developed.[30] This procedure can be classified into four distinctive steps:

(i) composing a dimensional matrix
(ii) partitioning the dimensional matrix
(iii) calculating additional matrices
(iv) forming the dimensional set.

Composing dimensional matrix

As the first step to assemble the dimensional variables from the list of dependent and independent variables into dimensionless groups, a dimensional matrix must be constructed. Table 4 shows the dimensional matrix for the dependent variable v_l and the independent variables P, γ, ΔT_o, c_p, k and ρ. Each row corresponds to a fundamental dimension, while each matrix element or cell contains the exponent of the fundamental dimensions of the variable. For example, P has a unit of Watt or in the fundamental dimensions, kg m^2 s^{-3}. As a result, under the P column in the dimensional matrix, the elements are 2 for length (m), 1 for mass (kg), -3 for time (s) and 0 for temperature (K). The elements in the dimensional matrix for the remaining variables can also be found in the same manner. Since v_l is the dependent variable, as a rule, it must be in the first or the leftmost column of the dimensional matrix.[30] The remaining columns represent the independent variables.

Partitioning dimensional matrix

The dimensional matrix in Table 4 must now be partitioned into matrix A and matrix B. This partitioning is necessary to allow the calculation of two additional matrices that will be required. Table 5 shows the partitioning of the dimensional matrix into matrix A and matrix B. Matrix A is a square matrix whose order is equal to the number of fundamental dimensions in the problem. In our example, there are four fundamental dimensions (i.e. kg, m, s and K). As a result, matrix A will be a 4×4 matrix. This square matrix is formed by selecting the four rightmost columns of the original dimensional matrix. Since the columns of matrix A represent four independent dimensional variables, these independent variables will be utilised repeatedly to form the foundation for each dimensionless group. Meanwhile, the remaining columns of the original dimensional matrix are used to form the matrix B.

In the current example, the columns of matrix A consist of the independent variables ΔT_o, c_p, k and ρ (*see* Table 4). This is one of the many possible forms of matrix A, since any four of the independent variables P, γ, ΔT_o, c_p, k and ρ can be used to create matrix A. In fact, during a typical dimensional analysis, different combinations of the independent variables are used in the formulation of matrix A. The final form of matrix A should allow an easy and meaningful physical interpretation of the resulting dimensionless groups. In addition, it is essential that matrix A has a non-zero determinant, since the inverse of matrix A will be used in a subsequent calculation. If the determinant of matrix A is zero, then the columns of the original dimensional matrix must be interchanged until a square matrix with non-zero determinant is found.

Table 4 Dimensional matrix of some of dependent and independent GMAW variables

	v_l	P	γ	ΔT_o	c_p	k	ρ
Length, m	1	2	0	0	2	1	−3
Mass, kg	0	1	1	0	0	1	1
Time, s	−1	−3	−2	0	−2	−3	0
Temperature, K	0	0	0	1	−1	−1	0

Table 5 Partitioning of original dimensional matrix in Table 4 into matrix A and matrix B

Matrix B			Matrix A			
1	2	0	0	2	1	−3
0	1	1	0	0	1	1
−1	−3	−2	0	−2	−3	0
0	0	0	1	−1	−1	0

Calculating additional working matrices

Once the original dimensional matrix has been partitioned, two new matrices are calculated before the assembly of the dimensionless groups. The first new matrix or matrix C is calculated using both matrices A and B and is based on the following equation

$$[C] = -\left([A]^{-1} \times [B]\right)^{T} \quad (21)$$

where [A], [B] and [C] are matrix A, B and C respectively. $[A]^{-1}$ is the inverse operation of matrix A while 'T' represents the matrix transpose operation. Using equation (4), matrix C in the present example is equal to

$$[C] = \begin{bmatrix} -0{\cdot}5 & -0{\cdot}5 & 0 & 0 \\ -0{\cdot}5 & 1{\cdot}5 & -2 & 1 \\ -0{\cdot}5 & 0{\cdot}5 & -1 & 0 \end{bmatrix} \quad (22)$$

The second additional required matrix, or matrix D, is a unit or identity matrix as shown in equation (23). This second matrix is a diagonal matrix with all non-zero elements equal to 1. Matrix D has the same number of rows as matrix C while its number of columns is the same as that of matrix B. Both new matrices are required to assemble the dimensionless groups

$$[D] = \begin{bmatrix} 1 & 0 & 0 \\ 0 & 1 & 0 \\ 0 & 0 & 1 \end{bmatrix} \quad (23)$$

Forming dimensional set

In the last step of the procedure, a dimensional set must be created. To create the dimensional set, matrices A and B are first recombined to form the original dimensional matrix (i.e. to undo the partitioning of the original dimensional matrix). Then, the identity matrix D is placed directly below matrix B while matrix C is positioned underneath matrix A. Thus, the dimensional set is an amalgamation of the original dimensional matrix and two new matrices that are strategically placed as illustrated in Table 6. The dimensional set consists of matrix B in the upper left corner, matrix A in the upper right corner, matrix D in the lower left corner and matrix C in the lower right corner. The combination of matrices D and C forms three new bottom rows of the dimensional set.

In this example, according to the Buckingham's theorem,[30] with seven dimensional variables and four fundamental dimensions, there will be three dimensionless groups: π_1, π_2 and π_3. The last three rows of the dimensional set in Table 6 contain the information that is used to assemble the dimensional variables together into various dimensionless groups. While the elements of the original dimensional matrix are the exponent of the dimension of each variable, the elements in the last three rows of the dimensional set are the exponent of the variables in the dimensionless groups. For example, from Table 6, the non-zero elements on the π_1 row correspond to v_l, ΔT_o, and c_p. The limiting welding speed has the exponent of 1 while ΔT_o and c_p have exponents of $-0{\cdot}5$. As a result, the first dimensionless group π_1 consists of v_l (i.e. exponent equals to 1) divided by the square root of the product of ΔT_o and c_p (i.e. exponents equal to $-0{\cdot}5$), i.e., $\pi_1 = v_l/(\Delta T_o \times c_p)^{1/2}$. The other two dimensionless groups π_2 and π_3 are determined in similar manners. The final overall results of this example of dimensional analysis are shown in equations (3)–(6).

Table 6 Combined set of dimensional set matrices [A], [B], [C] and [D]

	v_l	P	γ	ΔT_o	c_p	k	ρ
Length, m	1	2	0	0	2	1	−3
Mass, kg	0	1	1	0	0	1	1
Time, s	−1	−3	−2	0	−2	−3	0
Temperature, K	0	0	0	1	−1	−1	0
π_1	1	0	0	−0·5	−0·5	0	0
π_2	0	1	0	−0·5	1·5	−2	1
π_3	0	0	1	−0·5	0·5	−1	0

Acknowledgements

The present work was supported by Natural Sciences and Engineering Research Council of Canada (NSERC), Ontario Research and Development Challenge Fund (ORDCF) and its partners Alcan International, Babcock & Wilcox, Canadian Liquid Air Ltd, Centerline (Windsor) Ltd, John Deere, Magna International Inc., Ventra. Loan of robotic GMAW equipment by Lincoln Electric Company of Canada Ltd and Fanuc Robotics Canada Ltd is gratefully acknowledged. The TIME shielding gas used in the present study was supplied by BOC Gas.

References

1. H. B. Cary: 'Modern welding technology', 5th edn; 2002, Toronto, ON, Prentice Hall Canada Inc.
2. A. F. Manz: *Weld. J.*, 1990, **69**, (1), 67–68.
3. 'Welding handbook – Part 1: Welding processes', Vol. 2, 9th edn, 147–203; 2004, Miami, FL, American Welding Society.
4. K. A. Lyttle: *Weld. J.*, 1983, **62**, (3), 5–23.
5. Leonard. P. Connor: in 'Welding handbook', 8th edn, Vol. 1, 'Welding science and technology', 50; 1991, Miami, FL, American Welding Society.
6. in 'ASM handbook', Vol. 6, 'Welding, brazing and soldering', (ed. Davies *et al.*); 1993, Materials Park, OH, ASM International, 25.
7. R. L. O'Brien: in 'Welding handbook', 8th end, Vol. 2, 'Welding processes', 112–116; 1991, Miami, FL, American Welding Society.
8. T. C. Nguyen, D. C. Weckman, D. A. Johnson and H. W. Kerr: *Sci. Technol. Weld. Join.*, 2006, **11**, (6), 618–633.
9. E. Soderstrom and P. Mendez: *Sci. Technol. Weld. Join.*, 2006, **11**, (5), 572–579.
10. B. J. Bradstreet: *Weld. J.*, 1968, **47**, (6), 314s–322s.
11. K. Nishiguchi, K. Matsuyama, K. Terai and K. Ikeda: Proc. 2nd Int. Symp. on 'Advanced welding technology', Osaka, Japan, August 1975, Japan Welding Society, Paper 2-2-(10).
12. K. Nishiguchi and A. Matsunawa: Proc. 2nd Int. Symp. on 'Advanced welding technology', Osaka, Japan, August 1975, Japan Welding Society, Paper 2-2-(5).
13. T. C. Nguyen, D. C. Weckman, D. A. Johnson and H. W. Kerr: *Sci. Technol. Weld. Join.*, 2005, **10**, (4), 447–459.
14. T. Yamamoto and W. Shimada: Proc. 2nd Int. Symp. on 'Advanced welding technology', Osaka, Japan, August 1975, Japan Welding Society, Paper 2-2-(7).
15. W. F. Savage, E. F. Nipples and K. Agusa: *Weld. J.*, 1979, **58**, (7), 212s–224s.
16. S. Hiramoto, M. Ohmine, T. Okuda and A. Shinmi: Proc. Int. Conf. on 'Laser advanced material processing – science and application', Osaka, Japan, May 1987, High Temperature Society of Japan and Japan Laser Processing Society, 157–162.
17. C. E. Albright and S. Chiang: *J. Laser Appl.*, 1988, **1**, (1), 18–24.
18. S. Tsukamoto, H. Irie, M. Inagaki and T. Hashimoto: *Trans. Natl Res. Inst. Met.*, 1983, **25**, (2), 62–67.
19. S. Tsukamoto, H. Irie, M. Inagaki and T. Hashimoto: *Trans. Natl Res. Inst. Met.*, 1984, **26**, (2), 133–140.

20. M. Tomie, N. Abe and Y. Arata: *Trans. Japn. Weld. Res. Inst.*, 1989, **18**, (2), 175–180.
21. U. Gratzke, P. D. Kapadia, J. Dowden, J. Kross and G. Simon: *J. Phys. D*, 1992, **25D**, (11), 1640–1647.
22. P. F. Mendez and T. W. Eagar: Proc. 5th Int. Conf. on 'Trends in welding research', (ed. J. M. Vitek *et al.*), 13–18; 1998, Materials Park, OH, ASM International.
23. P. F. Mendez and T. W. Eagar: Proc. Conf. on 'Mathematical modelling of weld phenomena 5', (ed. H. Cerjak and H. K. D. H. Bhadeshia), 67–94; 2001, London, Institute of Materials.
24. P. F. Mendez and T. W. Eagar: *Weld. J.*, 2003, **82**, (10), 296s–306s.
25. T. C. Nguyen, D. C. Weckman and D. A. Johnson: submitted to *Weld. J.*, 2007, **86**, (11).
26. T. C. Nguyen: 'Weld defects in high-speed gas metal arc welding', PhD thesis, University of Waterloo, Waterloo, ON, Canada, 2005.
27. 'LaserStrobe model 4Z – Operation manual'; 1999, Idaho Fall, ID, Control Vision Inc.
28. S. B. Jones, J. Doherty and G. R. Salter: *Weld. J.*, 1977, **56**, (7), 19–31.
29. J. Biglou, D. C. Weckman, G. W. Bennett and H. W. Kerr: *Sci. Technol. Weld. Join.*, 2001, **6**, (1), 51–62.
30. T. Szires: 'Applied dimensional analysis and modeling'; 1998, Toronto, ON, McGraw-Hill.
31. H. E. Huntley: 'Dimensional analysis'; 1967, New York, Rinehart & Company Inc.
32. S. Subramanian and D. R. White: *Metall. Trans. B*, 2001, **32B**, 313–318.
33. S. M. Finlayson: 'Parametric modelling of high-speed gas metal arc welding', MASc thesis, University of Waterloo, Waterloo, ON, Canada, 2001.
34. R. D. Pehlke, A. Jeyarajan and H. Wada: 'Summary of thermal properties of casting alloys and mold materials', Report No. NSF/MEA-82028, NSF Applied Research Division, University of Michigan, Ann Arbor, MI, USA, 1982.
35. D. F. Watt, L. Coon, M. Bibby, J. Goldak and C. Henwood: *Acta Metall.*, 1988, **36**, (11), 3029–3035.
36. in 'The metals black book', (ed. J. E. Bringas), Vol. 1, 213–214; 1992, Edmonton, Alberta, Canada, CASTI Publishing Inc.
37. D. C. Weckman, H. W. Kerr and J. T. Liu: *Metall. Trans. B*, 1997, **28B**, (4), 687–700.